Original Article

Institution of MECHANICAL ENGINEERS
Journal of RAIL AND RAPID TRANSIT

Proc IMechE Part F:
J Rail and Rapid Transit
0(0) 1–13

DOI: 10.1177/09544097211030736
journals.sagepub.com/home/pif
SAGE

Quantification of vertical, lateral, and longitudinal fastener demand in broken spike track: Inputs to mechanistic-empirical design

Marcus S Dersch, Matheus Trizotto, J Riley Edwards and Arthur de Oliveira

Abstract

To address a recent challenge related to broken spikes in premium elastic fastening systems that have led to at least ten derailments and require manual walking inspections as well as build upon mechanistic-empirical (M-E) design principles for future fastening system component design, this paper quantifies the vertical, lateral, and longitudinal fastening system loads under revenue service traffic in a curve that has regularly experienced spike fastener fatigue failures. Previous data has indicated that the high rail of Track 3 experienced the most failures at this location. The data from this investigation sheds light into why failures are more predominant at this location than others and how the vertical, lateral, and longitudinal loads cannot be considered independently. Specifically, while the magnitude of the applied loading was the lowest on the high rail of Track 3, the threshold for failure was also the lowest given the operations at this location led to unloading of the high rail, thus indirectly highlighting the importance of friction within a fastening system. The data also show the high rail of Track 3 was subjected to the highest L/V load ratios and was an outlier in the typical lateral load reversals applied likely leading to spike stress reversals and thus a shorter fatigue life. Finally, based upon the data, it is recommended that to mitigate spike failures, as well as similar fastener challenges in other track types (e.g. rail seat deterioration, etc.) railroads should ensure trains operate close to the balance speed and use fastening system that transfer loads through friction. This study also provides novel data for M-E design of fastening systems.

Keywords

Fatigue failure, load characterization, fastening system design, longitudinal loads, operations, field data

Date received: 9 October 2020; accepted: 10 June 2021

Introduction

Approximately 94% of railroad track infrastructure worldwide is supported by ballast.[1] A ballasted track system consists of the rail, fastening systems, sleepers, ballast, sub-ballast, and subgrade.[2] Rail fastening systems, in conjunction with the sleeper, secure the rail to maintain gauge, transmit thermal and service loads, and anchor the rail-sleeper structure against lateral and longitudinal movements.[2] In doing so, fastening systems are required to transmit vertical, lateral, and longitudinal loads. As wheel loads and resulting forces transferred to the track structure have increased over time, and/or geometric tolerances become more stringent, fastening systems are required to perform more rigorous tasks (maintain tighter gauge, provide creep resistance, etc.).

To account for the increased forces and to address conditions symptomatic of track strength and force transfer deficiencies (e.g. plate cutting, rail seat deterioration (RSD), rail rollover, rail pad movement, etc.)[3] the fastening systems have evolved iteratively over time, through a trial-and-error design approach, like many other components in the rail infrastructure. These deficiencies have led to various track component failures (e.g. broken spikes, broken shoulders,

Rail Transportation and Engineering Center – RailTEC, Department of Civil and Environmental Engineering – CEE, Grainger College of Engineering – GcoE, University of Illinois at Urbana-Champaign – UIUC, 1240 Newmark Civil Engineering Laboratory, Urbana, IL, USA

Corresponding author:
Marcus S Dersch, Rail Transportation and Engineering Center – RailTEC, Department of Civil and Environmental Engineering – CEE, Grainger College of Engineering – GCoE, University of Illinois at Urbana-Champaign – UIUC, 1240 Newmark Civil Engineering Laboratory, MC-250, 205 N. Mathews Ave., Urbana, IL 61801, USA.
Email: mdersch2@illinois.edu

broken threaded rods, etc.) which have in-turn led to derailments.[4–9] Between 1999 and 2018 there have been 250 FRA-reportable train accidents in the United States that have resulted from "defective or missing spikes or rail fasteners" on mainlines and sidings as reported within the FRA Rail Equipment Accident or Incident Report (REAIR) 6180.54 database as discussed by Wang et al.[10] These failures demonstrate a disconnect between the loading demands placed on the track and strength of track components.

Fastener failures are not isolated to a single method of track construction (i.e. ballasted vs ballastless), nor are they isolated to the types of rolling stock with the highest loads. Force transfer fastener failures have been observed in ballasted sleeper track on heavy axle load (HAL) freight railroads as well as ballastless direct-fixation (DF) track systems used for heavy rail transit infrastructure. Furthermore, fastener failures are not caused by loads acting from a single direction (vertical, lateral, or longitudinal). Rather, most failures occur as a result of a combination of loads (vertical, lateral, and longitudinal).

While there has recently been increased modelling and laboratory testing of fastening system components,[11,12] the development and adoption of new fasteners has still relied heavily on practical experience and monitoring of revenue service field performance. This iterative method relying on field performance has led to inefficient designs and a lack of understanding of the underlying mechanisms that govern system response as a function of changing conditions (input loads, wear of components, support conditions, etc.) which has manifested itself in maintenance and safety problems; as is evident in the review of FRA track-caused accident data.

However, there has been a recent push to apply the principals of mechanistic-empirical (M-E) analysis design, currently used in pavement design,[13] to rail infrastructure component design. Initial suggestions for the application of a M-E analysis and design approach in the rail domain were documented by Van Dyk et al.,[14] Csenge et al.,[15] and Edwards et al.[16] These were further advanced by Quirós-Orozco[17] and Edwards,[18] leading to the development of a proposed framework for mechanistic-empirical analysis and design of railway track and its components.[19]

One of the first steps in the proposed M-E approach is to quantify the inputs of the system; track components, substructure depths, load environment, etc. Recent research has focused on quantifying vertical and lateral wheel loads on HAL freight, intercity passenger, and rail transit operations.[20–24] There has also been significant effort studying the key factors effecting the distribution of the vertical loads[2,25–27] and to a lesser extent the distribution of lateral loads to the supporting sleepers.[27–33] Finally, though there has been work quantifying longitudinal forces and displacements,[34–40] most studies have focused on quantifying absolute forces on structures or inputs to rail neutral temperature (RNT) models and not quantifying loads on fastening systems or individual rail seats; specifically as a result of a train pass. And once the loads are quantified and the track response is predicted through select models (e.g. fastener performance[11,41] or track behavior[27]) the outputs could be combined with track quality index (TQI) models[42,43] which forecast the deterioration of track given various track parameters (e.g. speed and tonnage).

Therefore, researchers from RailTEC at Illinois deployed instrumentation on a demanding revenue-service track that has experienced spike fastener fatigue failures previously to quantify the vertical, lateral, and longitudinal fastening system loading demands from HAL and empty freight traffic as well as passenger traffic. These data will both address a recent challenge related to broken spikes in timber sleeper elastic fastening systems that have led to at least ten derailments in the last twenty years and now require manual walking inspection to identify by quantifying loading conditions and build upon the M-E analysis and design foundation for future fastening system components.

Revenue service field site overview

Instrumentation was installed and data were collected on Tracks 1 and 3 within the full body of a 9.2-degree (623 ft (190 m)) curve located near Altoona, PA. The curve has three ballasted tracks constructed using timber sleepers and elastic fasteners with cut spikes. A visual walking-inspection identified one broken spike prior to instrumentation and tracks that appeared to be in a state-of-good-repair and thus representative of good maintenance practices, crosstie support, and components.

Figure 1 shows an overview of the revenue service field site, primary directions of traffic, generalized (expected) loading (empty vs loaded trains), and other relevant site information as well as the specific instrumentation deployed.

All tracks transport HAL freight and Amtrak intercity passenger trains. Freight operations consist of empty and loaded HAL unit trains, manifest trains, and intermodal trains loaded with containers and/or trailers. However, traffic direction and train type composition is biased for each track. Tracks 1 and 2 are primarily used by loaded freight trains operating downgrade while empty trains primarily operate upgrade on Track 3. Approximately 50 MGT of annual tonnage is accumulated on both Tracks 1 and 3 and they are on a 1.76% grade. Spike fatigue failures occur more frequently on Track 3 compared to Track 1 even though Track 1 transports comparatively more loaded trains. Further, as has been

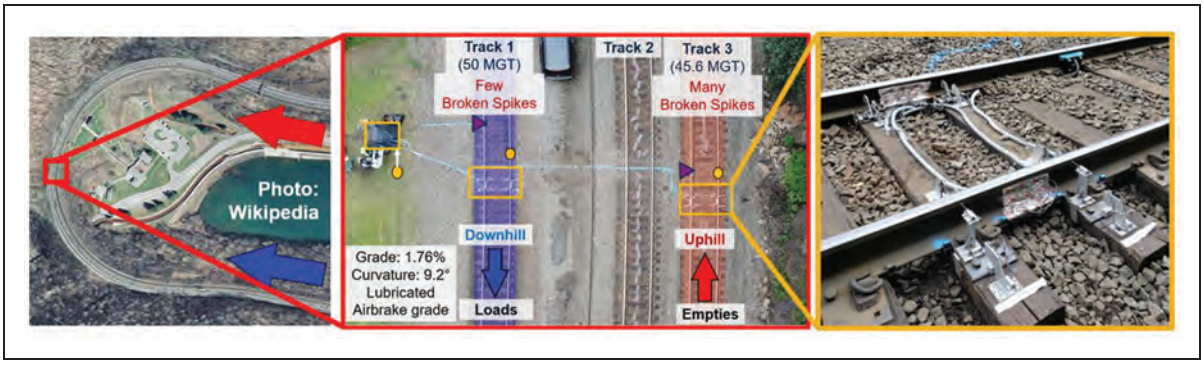

Figure 1. Aerial views of HAL field site with relevant track geometry and operations information (left and middle) and completed instrumentation on Track 3 of revenue service experimentation site (right).

documented elsewhere,[44,45] spike fatigue failure at this location primarily occurs on the high rail.

This location was selected because it provided an opportunity to quantify the forces placed on each track while limiting differences in track geometry (e.g. grade, curvature, etc.), climate, and weather. This facilitated isolation of the difference(s) leading to increased spike failures on the high rail of Track 3.

Instrumentation and data collection

Surface strain gauges were installed on the rail using industry-standard circuits and these circuits were calibrated using a loading frame. These calibrated circuits were used to quantify vertical, lateral, and longitudinal wheel-rail loads.[37,46] Additional instrumentation shown in Figure 1 was deployed as a part of broader research objective aimed at quantifying displacements but are not included within the scope of the current paper.

Vertical and lateral load circuits

Using the vertical load circuit, the voltages captured under passing wheels were transformed into vertical wheel forces using the calibration factors that were previously obtained. Next, peaks were pulled from the data and compared to the on-site commercially available RSR110 wheel sensor manufactured by Frauscher, to ensure all peaks were identified. Train speeds were estimated using the time between peaks and known locomotive wheelset distances.

To align with industry best practices, the maximum lateral load was quantified as the output from the lateral load circuit at the same timestamp as the application of maximum vertical wheel load. This is important given the signals of the lateral loads are not as consistent as the vertical load and are most reliable when the wheel is immediate over the center of the crib. Lateral forces were considered positive when acting in the direction of the field and negative when acting in the direction of the gauge. An example distance and time history of vertical and lateral load signals is shown in Figure 2.

Longitudinal circuits

Longitudinal rail forces were quantified using a circuit proposed by Harrison et al.[37] that includes that installation of gauges on both sides of the web of the rail at the neutral axis. To quantify the longitudinal rail force, the strains from the circuit are multiplied by the Young's modulus and cross-sectional area of the rail. This method does not allow for the identification of absolute rail axial loads since RNT is unknown but does facilitate the quantification of changes in rail load over time due to temperature changes and passing trains. The longitudinal load circuit does not show peaks under each passing wheel in the same way as the vertical and lateral circuits and requires additional insight to correctly interpret the results. Specifically, longitudinally induced strain from the bending of the rail under vertical and lateral loads overpower longitudinal strains under wheels, making readings inaccurate at those locations. Still, the method produces accurate measurements before the train's arrival, between the lead and trailing trucks, and after the passage of the train. For this project, longitudinal rail loads were taken at around 10-20 ft (3-6 m) in advance of the first wheel. To compensate for the offset, the measured rail loads are increased according to an exponential trend as described by Kerr[27] for a single wheel and more recently confirmed by Trizotto, et al (*Under review*) for multiple wheels. The superposition of multiple wheels was demonstrated to generate a median increase of 16%. Finally, results indicated that the longitudinal influence zone is significantly longer than what is observed from vertical and lateral load circuits (i.e. >100 ft (30.5 m) as compared to ~10 ft (3.05 m)) (Figure 3).

Data interpretation

A variety of methods were employed to quantify the demands placed on the fastening systems (e.g. rail seats) using wheel-rail forces that were obtained via rail circuits. The following sections detail the method and assumptions used to transform the wheel-rail

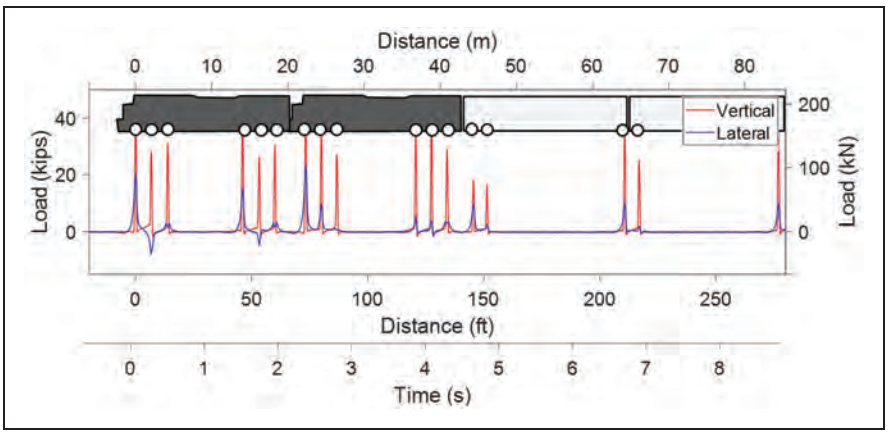

Figure 2. Example time history of vertical and lateral wheel loads.

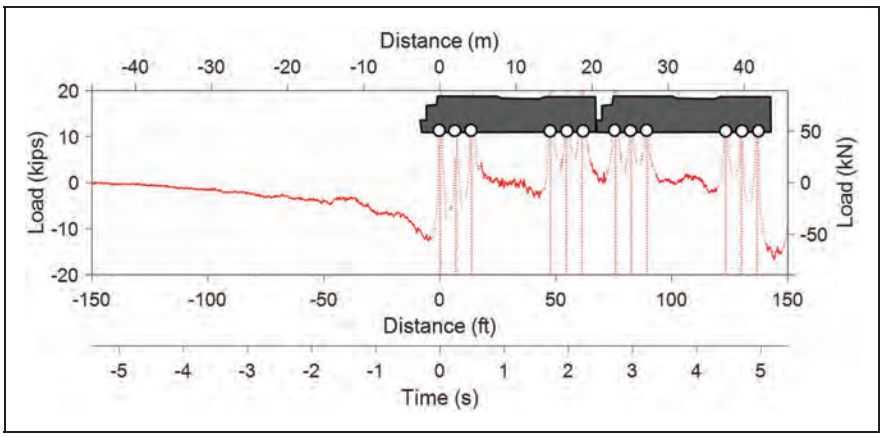

Figure 3. Example time history of longitudinal rail axial loads.

load data to rail seat load data. The methods provided below assume uniformly supported sleepers. The authors acknowledge that these assumptions might not account for the maximum stress a component would experience but have confidence that the loads are useful in relation to fatigue of components.

Vertical and lateral rail seat loads

Many analytical techniques have been developed for the quantification of vertical load distribution from multiple wheels to the supporting rail seats, many of which rely on beam on elastic foundation (BOEF) fundamentals. Some of the more recognizable developers of BOEF methods include Winkler, Talbot, and Zimmerman.[47–49] Winkler initially proposed a method based on BOEF theory that stated the reaction at longitudinal supports (e.g. each sleeper rail seat) was proportional to the rail deflection. Talbot and Zimmerman advanced this theory and validated it by comparing analytical results to field data.[47,49] While additional research in this topic has been completed, this foundational method is still widely used and is considered accurate for quantifying rail seat loads. Therefore, applying BOEF theory and assuming a timber sleeper track modulus of 3,500 lb./in./in. (24,270 kN/m/m), sleeper spacing of 19.5 in. (49.5 cm), axle spacing of 81.5 in. (207 cm), 136 RE rail (approximately UIC 60), and 36 in. (91 cm) wheel diameters, and superposition of adjacent wheels, the rail seat load would be 26% of the wheel load.

Vertical rail loads are influenced by multiple variables (e.g. speed of the train,[50] track modulus,[51] and wheel health). In this paper, the applied vertical rail loads are quantified by the instrumentation on the rail that account for these effects. Rail seat loads are also influenced by multiple variables (e.g. sleeper type, fastening system type, and sleeper support). The spike failures are not isolated to poorly supported sleepers given the widespread nature of what has been observed during field inspections (e.g. in one instance up to 10 sleepers in a row and in another instance 121 failed cut spikes (20% of potential spikes in a span of 150 sleepers on the high-rail of a single curve). Given that sleepers and fastening systems at this site were in good health, the authors assumed uniform sleeper

support. Thus, the relationship between the wheel-rail interface loads and rail seats loads was a fixed value.

Compared to vertical loads, there has been comparatively little research assessing the distribution of lateral loads to the fastening systems. The limited field observations and laboratory studies performed have indicated that lateral loads are distributed to fewer sleepers than vertical loads, thus increasing the maximum percentage of load felt by the center sleeper's rail seat (AREMA 2017). More specifically, studies on concrete sleepers have found that lateral rail seat loads range between 35 – 60% of the applied wheel load.[29,33] Given timber sleepers are less stiff than concrete sleepers, which has been partially offset using premium fastening systems, 35% lateral load transfer was selected for this study.

Longitudinal rail seat loads

Although longitudinal rail load and its distribution has been widely studied with respect to the field of RNT, no research has been aimed at quantified their distribution to the rail seats. Kerr[27] used analytical modeling to describe axial rail load and displacement due to a single longitudinal wheel load. This model uses a bar resting in a longitudinally elastic foundation, analogous to the BOEF method used for vertical load distribution. More elaborate, nonlinear FE models have been developed[52] and are even available in commercial software.[53] Despite these advancements, rail seat load distribution is not thoroughly described in the context of the loading demands on the fastening system components.

The analytical method developed by Kerr[27] and expanded by Trizotto et al.[54] quantifies longitudinal rail seat loads by assuming they are proportional to longitudinal rail displacement Equation (1) in the condition that there is no slip at the rail-fastener interface. Moreover, a parametric study was conducted to identify the effect of the superposition of multiple wheel loads and varying track stiffness. The model indicates that (in the elastic region) higher track stiffness (ballast + fastener stiffness) decreases the range of distribution of fastener and rail loads but increases individual fastener loads. Moreover, the superposition effect was found to be significant when multiple wheels are present. Regardless, increasing track stiffness resulted in increased fastener loading and reduced rail loading. The approach developed by Trizotto et al. (*Under review*) was used to quantify the rail seat loads in this study.

$$\underbrace{u(x) = \frac{R}{2\kappa EA} e^{-\kappa|x|}}_{\text{Rail Displacement}} \rightarrow \underbrace{f(x) = \frac{k_a}{2} u(x) = \frac{\kappa R}{2} e^{-\kappa|x|}}_{\text{Fastener Force per Unit Length}}$$
$$\text{with } \kappa^2 = \frac{k_a/2}{EA} \tag{1}$$

Where;
x = location, in relation to the wheel load,
$u(x)$ = rail section displacement at location x,
$f(x)$ = fastener force per unit length at location x,
R = longitudinal wheel load, per rail,
$k_a/2$ = longitudinal track stiffness, per rail,
E = Young's modulus of the rail, and
A = cross-sectional area of the rail.

Longitudinal track stiffness varies longitudinally due to variation in ballast condition, spike engagement on the fastener, and magnitude of vertical loads.[55] Since the longitudinal modulus of the tracks studied are unknown, a representative (and conservative) longitudinal track modulus of 3,000 lb./in./in. (20,800 kN/m/m) was selected for both tracks. This value is comparable to measured longitudinal modulus of vertically loaded ballasted track sections[38] and is believed to bound actual field conditions. Further, Trizotto et al.[54] found that while there is a direct nonlinear relationship between longitudinal track modulus and fastener loads, a quadrupling of modulus was required to see a 30% increase in fastener load. Therefore, it is reasonable to believe that any small changes in longitudinal track modulus will have a small effect on the longitudinal fastener loads.

The method used in this paper involves estimating the rail and fastener load distribution for the given longitudinal track stiffness, uniform wheel loads, and each train's approximate wheel configuration. It considers leading locomotives for uphill and downhill trains and additional cars following the locomotives for downhill trains (to simulate the contribution of all braking axles). Since it is assumed that loads are in the elastic region, these distributions are linearly proportional to the applied wheel loads. Therefore, the distributions are scaled to match the rail axial loads at the first passing wheel and the maximum rail seat load is recorded.

Results

The following sections document the vertical, lateral, and longitudinal wheel-rail and fastener forces and the role they play in spike fatigue failures. Data were recorded on both tracks for a period of nine days. Over 50 train passes were recorded on each track during this period. Only freight trains were considered in the analysis and due to the biased directionality of traffic a comparison is made between trains on Track 1 going downhill and trains on Track 3 going uphill; representing the dominant directions for traffic.

The speeds of the trains were quantified, using the method described previously, and indicate the trains operated at median speeds of 18 and 17 mph (29 and 27 kph) on Tracks 1 and 3, respectively (Figure 4). Given the geometry of the curve (4" (10.2 cm) nominal superelevation and 9.2 degree (623 ft (190 m)) curve), the balanced speed for both tracks was

calculated to be 25.5 mph (41 kph). Therefore, the data indicate that most trains were operating below balance speed. Further, over this range of speeds, the impact of speed on dynamic loading would be minimal as shown by Sadeghi[56] and Van Dyk.[50]

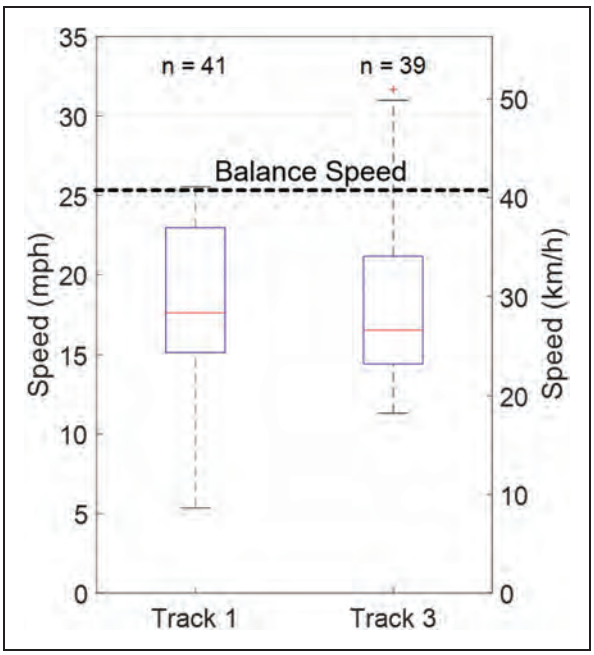

Figure 4. Measured speed of trains on Tracks 1 and 3 in July 2019.

Vertical loading

Utilizing the methods described previously, vertical rail loads and corresponding vertical rail seat loads were quantified (Figure 5). As expected, the vertical demands on Track 1 are significantly greater than Track 3. Median vertical rail seat loads were 7.5 and 7.8 kips (33.4 and 34.7 kN) (high and low rails, respectively) on Track 1 and 2.8 and 4.3 kips (12.5 and 19.1 kN) (high and low rails, respectively) on Track 3. Therefore, the high and low rails of Track 1 are subjected to 4.7 and 3.5 kips (29.1 and 15.6 kN) more vertical force than Track 3, respectively.

While there is a convergence of loading between both rails on Track 1 and the low rail of Track 3 at higher percentiles (i.e. >90%) (likely accounting for the locomotives and loaded trains), there is consistently a lower vertical demand on the high rail of Track 3. This unbalance in loads between the high and low rails, aligns with expectations given the operations and balance speed.[57] However, the balance seen in Track 1 indicates either a deviation in actual track geometry from the track charts or an effect of train handling down the grade. It is hypothesized that the underbalanced operations leading to this lower magnitude vertical rail seat load (median value of 2.8 kips (13 kN)) leads to a reduction in frictional capacity at the plate to sleeper interface on the high rail of Track 3 and plays a role in the increased spike failure. Therefore, lower longitudinal or lateral loads would be required to exceed the frictional resistance and transfer additional loads to the spikes.

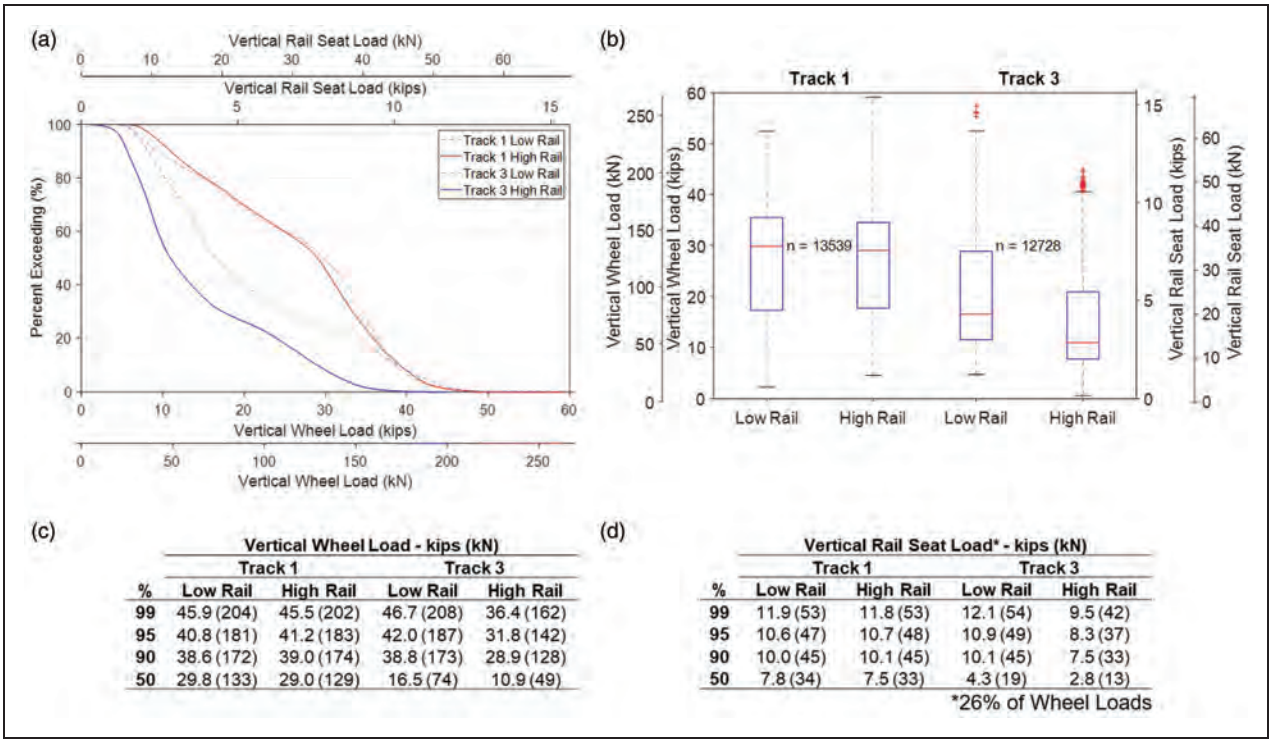

Figure 5. Quantitative data for vertical wheel loads ((a) percent exceedance (b) box-plots and (c) load values at select percentiles table) and rail seat loads ((d) rail seat load values at select percentiles table) for both high and low rails of both tracks.

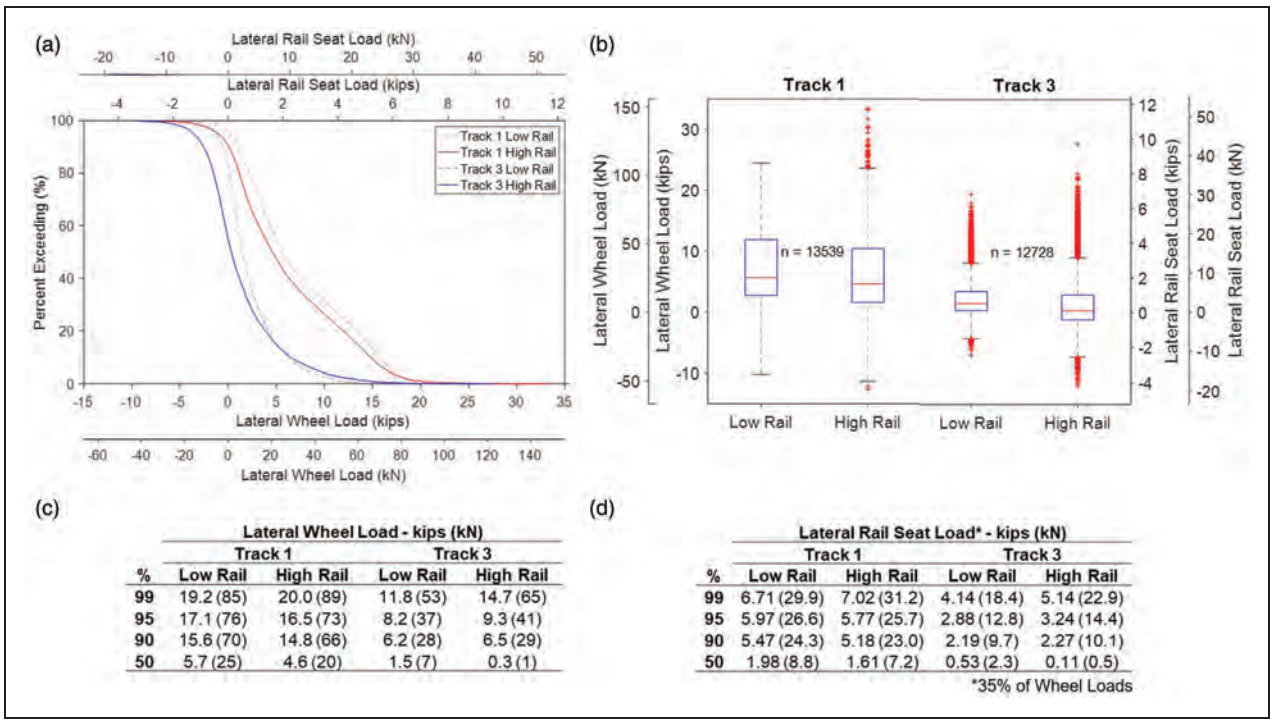

%	Track 1 Low Rail	Track 1 High Rail	Track 3 Low Rail	Track 3 High Rail
99	19.2 (85)	20.0 (89)	11.8 (53)	14.7 (65)
95	17.1 (76)	16.5 (73)	8.2 (37)	9.3 (41)
90	15.6 (70)	14.8 (66)	6.2 (28)	6.5 (29)
50	5.7 (25)	4.6 (20)	1.5 (7)	0.3 (1)

%	Track 1 Low Rail	Track 1 High Rail	Track 3 Low Rail	Track 3 High Rail
99	6.71 (29.9)	7.02 (31.2)	4.14 (18.4)	5.14 (22.9)
95	5.97 (26.6)	5.77 (25.7)	2.88 (12.8)	3.24 (14.4)
90	5.47 (24.3)	5.18 (23.0)	2.19 (9.7)	2.27 (10.1)
50	1.98 (8.8)	1.61 (7.2)	0.53 (2.3)	0.11 (0.5)

Figure 6. Quantitative data for lateral wheel loads ((a) percent exceedance (b) box-plots and (c) load values at select percentiles table) and rail seat loads ((d) rail seat load values at select percentiles table) for leading and trailing axles on both high and low rails for both tracks.

Lateral loading

Utilizing the methods described previously the lateral rail loads and corresponding lateral rail seat loads were quantified (Figure 6). As expected, the lateral demands on Track 1 are significantly greater than Track 3. Median lateral rail seat loads were 1.61 and 1.98 kips (7.2 and 8.8 kN, respectively) (high and low rails, respectively) on Track 1 and 0.11 and 0.53 kips (0.5 and 2.5 kN, respectively) (high and low rails, respectively) on Track 3. Therefore, the high and low rails of Track 1 are subjected to 1.50 and 1.45 kips (6.7 and 6.5 kN, respectively) more lateral force than Track 3, respectively. However, the high rail of Track 3 is an outlier in that loads generated from trailing axles are most often gage facing as opposed to the more common application of loads toward the field. Therefore, it is the only rail that would regularly be subjected to reverse lateral loads (i.e. alternating field and gage facing). This reversal of load could lead to increased movement of the fastening system and greater fastener component stress ranges. Additionally, when considering fatigue, load reversals lead to a decrease in fatigue life.[58]

The applied lateral to vertical (L/V) load ratio is a numerical ratio of lateral load applied at a point on the rail to the vertical load applied at that same point.[59] Though commonly considered a metric for determining the risk of derailment (e.g. wheel-climb or rail-rollover), L/V is commonly increased during laboratory testing to represent more severe environments.[60,61] Hay[2] indicates that 0.68 is the threshold in which the rail becomes unstable due to the resultant L and V force passing outside the rail base. Further, though the metric represent the loads applied at the wheel-rail interface, a rail seat L/V (i.e. representing the loads applied at the rail seat) could be more representative of what the fastener would be subjected while also aligning more with the AREMA[60] recommendation which considers L/V ratios above 0.52 to be severe service. The rail seat L/V would be 35% higher than what is seen at the wheel-rail interface, accounting for the parameters previously discussed in this paper (i.e. the vertical and lateral load percentages transferred to the rail seat beneath the point of load application are 26 and 35%, respectively. Table 1 provides the wheel-rail and rail seat L/V ratios for the leading axles of Tracks 1 and 3.

The observed wheel-rail L/V ratios were greatest on the high rail of Track 3 and ranged from −0.44 to 0.72 (1st percentile to 99th percentile, respectively). The field side L/V of 0.72 exceeds the threshold proposed by Hay (0.68) indicating that the high rail of Track 3 could be unstable. The 95th percentile rail seat L/V ratios of all rails exceeded the 0.52 threshold recommended by AREMA in Chapter 30 (Ties) for design qualification testing.[60] Track 3 was subjected to L/V magnitudes that were 50% greater at the 95th percentile (0.78) and 87% greater at the 99th percentile (0.97) as compared to the 0.52 threshold. Previous

Table 1. Wheel-rail and rail seat L/V ratios of leading axles of the high and low rails on tracks 1 and 3.

Wheel rail L/V					Rail seat rail L/V				
	Track 1		Track 3			Track 1		Track 3	
Percentile	Low	High	Low	High	Percentile	Low	High	Low	High
99	0.54	0.56	0.48	0.72	99	0.73	0.75	0.65	0.97
95	0.50	0.50	0.39	0.58	95	0.67	0.67	0.53	0.78
90	0.48	0.46	0.34	0.49	90	0.64	0.63	0.46	0.65
50	0.36	0.34	0.12	0.17	50	0.48	0.46	0.17	0.23
10	0.15	0.21	0.03	–0.19	10	0.21	0.28	0.04	–0.25
5	0.11	0.17	0.00	–0.27	5	0.15	0.23	0.00	–0.36
1	–0.01	0.08	–0.05	–0.44	1	–0.01	0.11	–0.07	–0.59

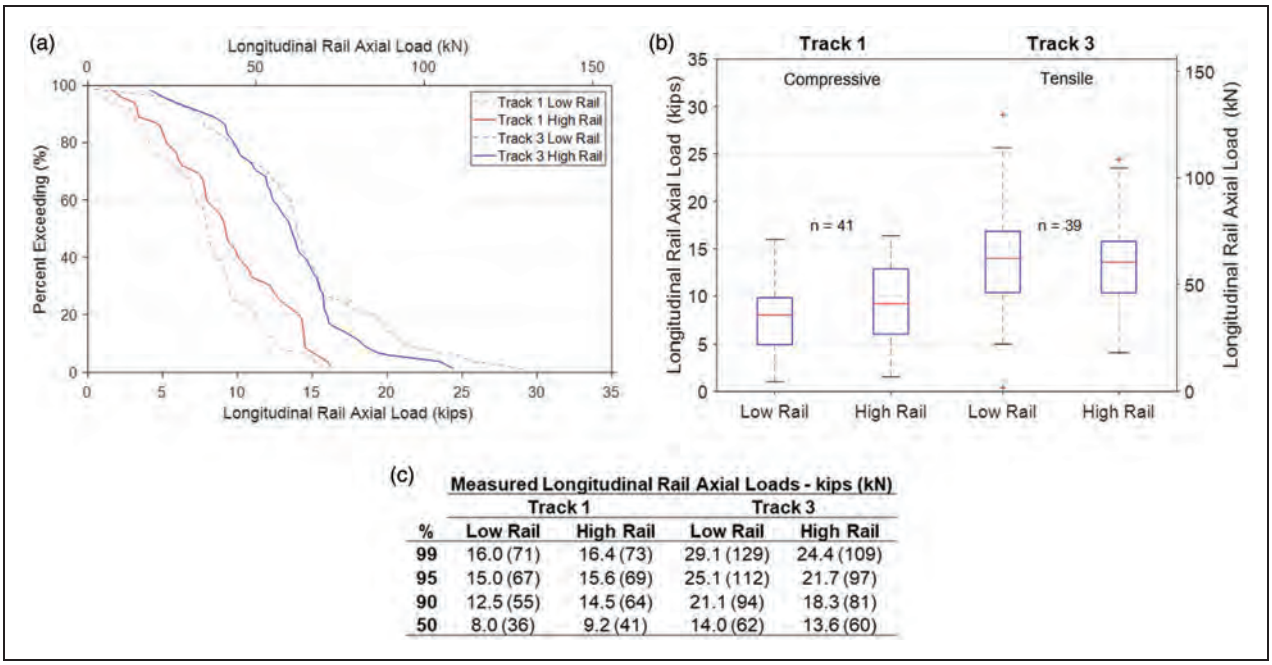

Figure 7. Quantitative data ((a) percent exceedance (b) box-plots and (c) load values at select percentiles table) for longitudinal wheel loads for both high and low rails.

research by Kerchof[62] showed that excess elevation leads to increased L/V load ratios on the high rail and increased gauge widening. Therefore, reducing the elevation of the curve and balancing the forces has already been shown to improve track health and thus could also be expected to mitigate spike failures.

Longitudinal loading

Measured longitudinal rail loads are presented in Figure 7, showing that the mean tensile rail loads were greater on Track 3 than Track 1. The rail seat loads on each track are presented in Figure 8. Results indicate that longitudinal rail seat loads are at least an order of magnitude lower than the longitudinal wheel loads (i.e. <10%). Moreover, the longitudinal demands on Track 3 are greater than the loads imparted on Track 1. The median longitudinal rail seat loads were 0.97 and 0.84 kip (4.3 and 3.7 kN, respectively) (high and low rails, respectively) on Track 1 and 1.29 and 1.39 kips (5.7 and 6.2, respectively) (high and low rails, respectively) on Track 3. Therefore, the high and low rails of Track 1 are subjected to 0.32 and 0.55 kips (1.4 and 2.4 kN, respectively) lower longitudinal force than Track 3, respectively.

Research has shown that a single spike could be subjected to 70% of the applied rail seat load given the likely non-uniform distribution amongst the spikes within a single rail seat.[63,64] Considering this, only the 99th percentile longitudinal load on the low rail of Track 3 exceeds the minimum load required to produce spike fatigue failures of 2,000 lb. (8.9 kN) according to Dersch et al.[41] Therefore, the data indicate that there must be a combination of both lateral and longitudinal loads transferred to the spikes to lead to spike fatigue failures.

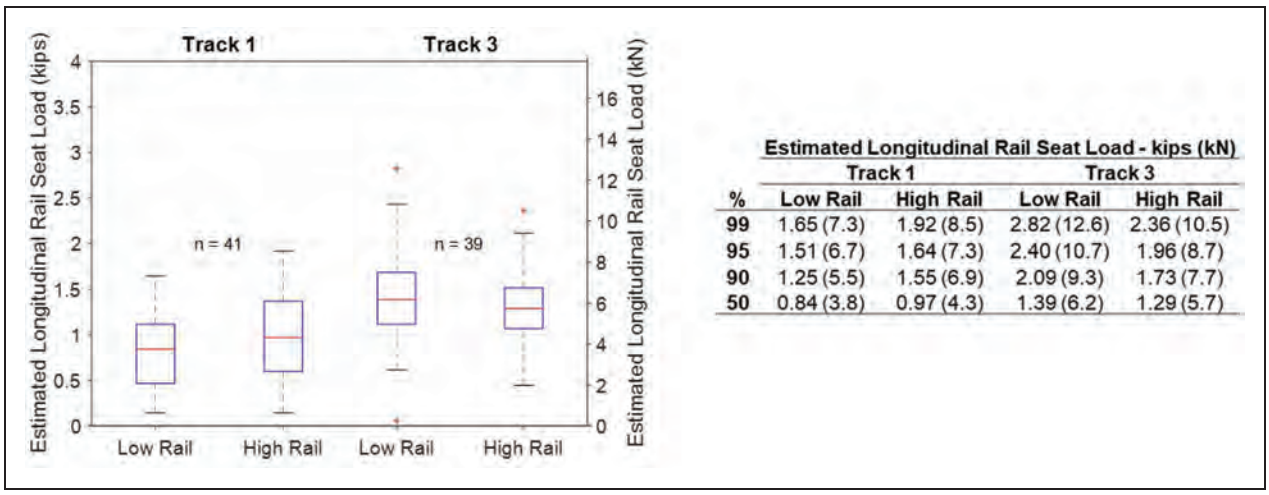

Estimated Longitudinal Rail Seat Load - kips (kN)				
	Track 1		Track 3	
%	Low Rail	High Rail	Low Rail	High Rail
99	1.65 (7.3)	1.92 (8.5)	2.82 (12.6)	2.36 (10.5)
95	1.51 (6.7)	1.64 (7.3)	2.40 (10.7)	1.96 (8.7)
90	1.25 (5.5)	1.55 (6.9)	2.09 (9.3)	1.73 (7.7)
50	0.84 (3.8)	0.97 (4.3)	1.39 (6.2)	1.29 (5.7)

Figure 8. Quantitative data for longitudinal rail seat loads for both high and low rails.

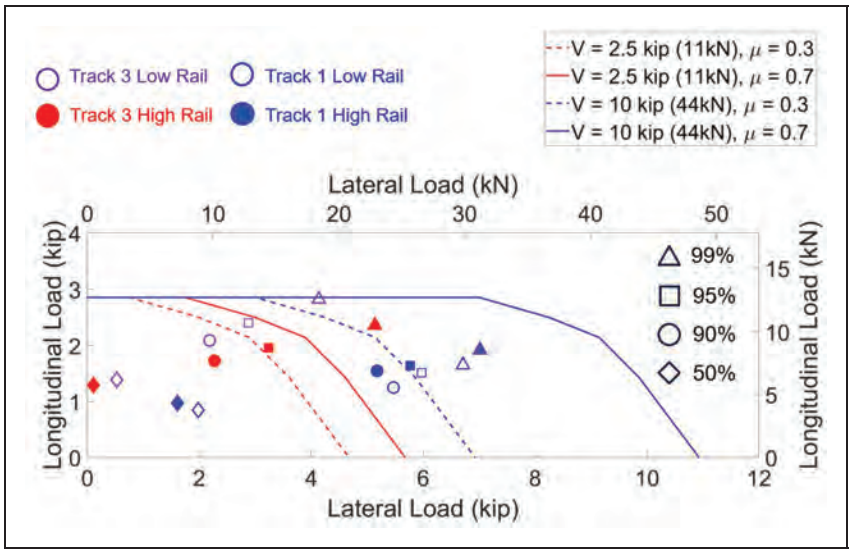

Figure 9. Effect of rail seat vertical load and plate to sleeper friction on total spike load for various lateral and longitudinal rail seat load combinations with failure threshold identified.

Total spike demands considering timing of load application and frictional effects

When considering the combined effect of longitudinal and lateral loads, the timing of load application and quantification of the friction at the plate-sleeper interface is critical. As discussed previously, the longitudinal load zone of influence is significantly greater than either vertical or lateral. Further, the wave action of the rail ahead of a wheel is known to produce rail uplift,[47] as predicted by BOEF models.[27] It is therefore reasonable to assume that the longitudinal loads are applied when there is rail uplift, directly bearing on the spikes (e.g. not carried by friction). Further, based on the sequence of load application, the lateral loads would be applied when there is contact between the plate-sleeper and thus resisted by friction and spike bearing.

The median, 90th, 95th, and 99th lateral and longitudinal rail seat loads from all rails were transformed into spike loads using equations (2) and (3) below, which is similar to the load severity calculation as presented by FRA.[59] Coefficients of friction (μ) between timber and steel can vary from 0.3 and 0.7 depending on moisture content of the timber, surface treatment, or roughness of the plate.[65] The resulting lateral and longitudinal spike loads are plotted in Figure 9 as are the spike endurance limit thresholds for the given rail seat vertical load and μ.

$$P_{Spike,\ Long} = 0.7 \cdot F_{Long} \tag{2}$$

$$P_{Spike,\ Lat} = \begin{cases} 0.7(F_{Lat} - \mu \cdot F_{Vert}) & if\ |F_{Lat}| > \mu \cdot F_{Vert} \\ 0 & if\ |F_{Lat}| \leq \mu \cdot F_{Vert} \end{cases} \tag{3}$$

Where
F_{Vert} = Fastener vertical load (≥ 0)
F_{Lat} = Fastener lateral load
F_{Long} = Fastener longitudinal load

$P_{Spike,\ Lat}$ = Spike lateral load

$P_{Spike,\ Long}$ = Spike longitudinal load

Field data indicate that fatigue failures could be expected on either track when friction is low. However, as friction increases, fewer failures would be expected given the load required to exceed the failure threshold increases. Considering the vertical load data at this location, the high rail of Track 3 (median vertical rail seat load of 2.8 kips (12.5 kN)) is closest to the lower bound vertical applied load (2.5 kips (11.1 kN)), as presented. However, the low rail of Track 3 and both rails of Track 1 would have failure thresholds closer to the upper bound vertical load (10 kips (44.5 kN)), as shown in Figure 9. Therefore, this data indicate that while the magnitude of lateral and longitudinal applied loads on the high rail of Track 3 is the lowest, the threshold for failure is also the lowest and at reasonable friction levels, more failures would be expected on the high rail of Track 3, which aligns with actual field performance.

Conclusions

To address a recent challenge related to broken spikes in premium elastic fastening systems that have led to at least ten derailments and require manual inspection as well as build upon the M-E analysis and design foundation for future fastening system component design this paper quantifies the vertical, lateral, and longitudinal fastening system loads. The revenue service field data were collected at a curved location on a freight railroad that has historically experienced fatigue failed spikes.

In summary, this investigation showed that while the magnitude of the applied vertical load was the lowest on the high rail of Track 3 (the location of the majority of failures), the threshold for failure is also the lowest given the lower magnitude vertical rail seat load reduced the frictional load capacity to a level that was exceeded more often than on Track 1. The data also showed the high rail of Track 3 was subjected to the highest L/V load ratios and was in outlier in the typical lateral load reversals applied in which likely would lead to a reversal in stress in the spike and thus shorter fatigue life. A summary of additional findings from this investigation include:

- For a given wheel load, the maximum vertical, lateral, and longitudinal load percentage transferred to the fastening system was approximately 26%, 35%, and <10%, respectively
- Underbalance operations led to a median rail seat vertical load of 2.8 kips (12.5 kN) on the high rail of Track 3 and thus the lowest friction capacity of all rail seats
  - The higher magnitude vertical loads on both rails of Track 1 and the low rail of Track 3 provide greater frictional resistance as compared to the high rail on Track 3, likely reducing the amount of load transferred into the spikes.

- Longitudinal fastener loads ranged from 1.29 to 2.40 kips (5.8 to 10.7 kN) for Track 3 and 0.84 and 1.64 kips (3.7 to 7.3 kN) for Track 1 for the nominal and 95% loads, respectively.
- Lateral fastener loads ranged from 0.11 to 2.88 kips (0.5 to 12.8 kN) for Track 3 and 1.61 and 5.97 kips (7.1 to 26.6 kN) for Track 1 for the nominal and 95% loads, respectively.
- The 95th percentile rail seat L/V ratio of 0.78 on the high rail of Track 3 is 50% greater than the 0.52 values fastening systems are subjected to during severe service testing as recommended by AREMA.
- Spike fatigue failures are driven through a combination of both lateral and longitudinal loading.
  - The longitudinal load magnitudes, which are present even when vertical and lateral loads are not applied, are insufficient to independently cause fatigue failures.

To mitigate spike failures at this location, as well as similar failures in other track types (e.g. rail seat deterioration, etc.) railroads should ensure operations are as close to the balance speed of track as possible. This would increase the vertical force on the high rail of Track 3 while reducing the L/V ratios and lateral load reversal. Finally, encouraging friction between the plate and sleeper is critical in reducing the forces transferred to the spike.[66]

Authors' contribution

The authors confirm contribution to the paper as follows: study conception and design: Marcus Dersch, Arthur Lima, Matheus Trizotto, and J. Riley Edwards; data collection: Marcus Dersch, Matheus Trizotto, Arthur Lima; analysis and interpretation of results: Marcus Dersch, Matheus Trizotto, and J. Riley Edwards; draft manuscript preparation: Marcus Dersch, Matheus, Trizotto, J. Riley Edwards. All authors reviewed the results and approved the final version of the manuscript.

Acknowledgements

The material in this paper represents the position of the authors and not necessarily that of sponsors. The authors also would like to thank Brad Kerchof for his continued insight and comments related to broken. Finally, the

authors acknowledge the following project industry partners for supplying insight, recommendations, and materials to this study: NS; CN; CSX; BNSF; Union Pacific; Volpe Center; Cossloh North America; Progress Rail; Evertrak; Lewis Bolt and Nut; and Pandrol USA. J. Riley Edwards has been supported in part by the grants to the UIUC Rail Transportation and Engineering Center (RailTEC) from CN and Hanson Professional Services.

Declaration of Conflicting Interests

The author(s) declared no potential conflicts of interest with respect to the research, authorship, and/or publication of this article.

Funding

The author(s) disclosed receipt of the following financial support for the research, authorship, and/or publication of this article: This research effort is funded by the Federal Railroad Administration (FRA), part of the United States Department of Transportation (US DOT). This work was also supported by the National University Rail Center, a U.S. Department of Transportation Office of the Assistant Secretary for Research and Technology Tier 1 University Transportation Center.

ORCID iDs

Marcus S Dersch https://orcid.org/0000-0001-9262-3480
J Riley Edwards https://orcid.org/0000-0001-7112-0956
Arthur de Oliveira https://orcid.org/0000-0002-9642-2931

References

1. Matias SR and Ferreira PA. Railway slab track systems: review and research potentials. *Struct Infrastruct Eng* 2020; 16: 1635–1653.
2. Hay WW. Chapter 15: track analysis. In: *Railroad engineering*. Hoboken, NJ, USA: John Wiley & Sons, 1982, pp.239–275.
3. Kerr AD III. The evolution of track components. In: *Fundamentals of railway track engineering*. Omaha, NE: Simmons Boardman, 2003, pp.25–84.
4. Choros J, Coltman MN and Marquis B. Prevention of derailments due to concrete tie rail seat deterioration. In: *Proceedings of the 2007 joint rail conference and internal combustion engine division spring technical conference*. Pueblo, CO: American Society of Mechanical Engineers (ASME), New York: NY, 2007. pp.173–181.
5. Edwards JR, Chavez L, Qian Y, et al. *Field study and analytical modeling of the performance of existing WMATA anchor bolt system*. Final Report CQ17066, Washington, DC, USA: Washington Metropolitan Area Transit Authority, 2018.
6. McHenry M and LoPresti J. *Tie and fastener system gage restraint performance at FAST*. TD-15-013. Pueblo, CO: Association of American Railroads, Transportation Technology Center, Inc., 2015.
7. Roadcap T, Kerchof B, Dersch MS, et al. Field experience and academic inquiry to understand mechanisms of spike and screw failures in railroad fastening systems. In: *Proceedings of the 2019 AREMA annual conference with railway interchange*. Minneapolis, MN: AREMA, 2019.
8. Wolf GP. Effects of wide gauge on derailment potential. In: *Proceedings of 2014 wheel rail interaction heavy haul seminar*, Chicago, IL, USA, January 2014, p. 4. Chicago: IL.
9. Wu H and Kerchof B. Management of wheel/rail interface to prevent rail rollover derailments. *Proc IMechE, Part F: J Rail and Rapid Transit* 2014; 228: 673–686.
10. Wang BZ, Barkan CP and Rapik Saat M. Quantitative analysis of changes in freight train derailment causes and rates. *J Transp Eng, Part A: Systems* 2020; 146: 04020127.
11. Sadeghi J, Seyedkazemi M and Khajehdezfuly A. Nonlinear simulation of vertical behavior of railway fastening system. *Eng Struct* 2020; 209: 110340.
12. Sadeghi J, Fesharaki M and Khajehdezfuly A. Influences of train speed and axle loads on life cycle of rail fastening clips. *Trans Can Soc Mech Eng* 2015; 39: 1–11.
13. American Association of State Highway and Transportation Officials (AASHTO). *Mechanistic-empirical pavement design guide*. Washington, DC: American Association of State Highway and Transportation Officials (AASHTO), 2008.
14. Van Dyk BJ, Edwards JR, Ruppert CJ Jr, et al. Considerations for mechanistic design of concrete sleepers and elastic fastening systems in North America. In: *Proceedings of the 10th international heavy haul association conference*, New Delhi, India, 4–6 February 2013, http://railtec.illinois.edu/CEE/pdf/Conference%20Proceedings/2013/Van%20Dyk%20et%20al%202013.pdf (2013, accessed 28 March 2017).
15. Csenge MV, Lin X, Wolf H, et al. Mechanistic design of concrete monoblock crossties for rail transit loading conditions. In: *Proceedings of the 2015 APTA rail conference*. Salt Lake City, UT: American Public Transportation Association (APTA), 2015.
16. Edwards JR, Dersch MS and Kernes RG. *Improved concrete crosstie and fastening systems for US high speed passenger rail and joint Corridors – technical report (volume 2)*. Washington, DC: Federal Railroad Administration (FRA), 2017.
17. Quirós-Orozco RJ. *Prestressed concrete railway crosstie support variability and its effect on flexural demand*. Master's Thesis, University of Illinois at Urbana-Champaign, Department of Civil and Environmental Engineering, 2018.
18. Edwards JR. *Quantification of prestressed concrete railway crosstie flexural response: implications for mechanistic design*. Doctoral Thesis, University of Illinois at Urbana-Champaign, Department of Civil and Environmental Engineering, 2019.
19. Edwards JR, Quirós-Orozco RJ, Bastos JC, et al. Vision for mechanistic-empirical railway track system and component analysis and design. *Transp Res Rec J Transp Res Board* in review; 20: 1–15.
20. Edwards JR, Cook A, Dersch MS, et al. Quantification of rail transit wheel loads and development of improved dynamic and impact loading factors for design. *Proc IMechE, Part F: J Rail and Rapid Transit* 2018; 232: 2406–2417.
21. Lin X, Edwards JR, Dersch MS, et al. Load quantification of the wheel–rail interface of rail vehicles for the infrastructure of light rail, heavy rail, and commuter

rail transit. *Proc IMechE, Part F: J Rail and Rapid Transit* 2018; 232: 596–605.
22. Quirós-Orozco RJ, Edwards JR, Qian Y, et al. Quantification of loading environment and flexural demand of prestressed concrete crossties under shared corridor operating conditions. *Transport Res Record* 2018; 2672: 136–145.
23. Van Dyk BJ, Dersch MS, Edwards JR, et al. Load characterization techniques and overview of loading environment in North America. *Transport Res Record* 2014; 2448: 80–86.
24. Van Dyk BJ. *Characterization of the loading environment for shared-use railway superstructure in North America*. Master's Thesis, University of Illinois at Urbana-Champaign, Department of Civil and Environmental Engineering, www.ideals.illinois.edu/handle/2142/72855 (2014, accessed 10 March 2017).
25. Eisenmann J. Stress distribution in the permanent way due to heavy axle loads and high speeds. In: *Proceedings of the 69th annual convention of the American Railway Engineering Association (AREA)*. Chicago, IL, USA: AREA, pp.24–59.
26. Hasan N. Railroad tie spacing related to wheel-load distribution and ballast pressure. *Pract Period Struct Des Constr* 2015; 20: 04014047.
27. Kerr AD. IVResponse of track to wheel loads. In: *Fundamentals of Railway Track Engineering*. Omaha, NE: Simmons Boardman, 2003, pp.84–134.
28. Deshimaru T, Tamagawa S and Kataoka H. Permissible lateral force and fatigue life for rail fastening system. *Q Rep RTRI* 2017; 58: 236–241.
29. Holder BG, Qian Y, Dersch MS, et al. Lateral load performance of concrete sleeper fastening systems under non-ideal conditions. In: *Proceedings of the 11th international heavy haul association conference*, Cape Town, South Africa, 2–6 September 2017.
30. Holder DE, Csenge MV, Qian Y, et al. Laboratory investigation of the SKL-style fastening system's lateral load performance under heavy haul freight railroad loads. *Eng Struct* 2017; 139: 71–80.
31. Kish A. On the fundamentals of track lateral resistance. In: *American railway engineering and maintenance-of-way-association annual conference*, Minneapolis, MN, USA, 18–21 September 2011. p. 45. AREMA: Chicago, IL.
32. Shenton HW III. Analysis of crosstie track in lateral plane using new track equations. *J Transp Eng* 1997; 123: 202–208.
33. Williams BA, Holder D, Edwards JR, et al. Quantification of the lateral forces in concrete sleeper fastening systems. *Proc IMechE, Part F: J Rail and Rapid Transit* 2016; 230: 1714–1721.
34. Ahmad SSN, Mandal NK, Chattopadhyay G, et al. Improvement of rail creep data to measure the stress state of a tangent continuously welded rail (CWR) track. In: *Proceedings of the 2011 international heavy haul association conference*, Calgary, Canada, 19–22 June 2011, p. 8. IHHA: Virginia Beach, VA.
35. Bose T, Levenberg E and Zania V. Analyzing track responses to train braking. *Proc IMechE, Part F: J Rail and Rapid Transit* 2018; 232: 1984–1993.
36. El-Sibaie M and Anderson G. *Measurement of rail forces and displacements under AC-Traction and DC-Traction locomotives*. Technical R-869, Chicago, IL: Association of American Railroads, Chicago Technical Center, 1994.
37. Harrison H, Sluz A and Clark D. Monitoring CWR longitudinal force behavior using remote sensing technology. In: *International Conference on Innovations in the Design & Assessment of Railway Track*. Delft, Netherlands, 2–3 December 1999.
38. Kerokoski O. Determination of longitudinal and transverse railway track resistance. In: 2010 *Joint Rail Conference*, Volume 1. Urbana, IL: ASMEDC, pp.157–165.
39. Kish A and Samavedam G. *Longitudinal force measurement in continuous welded rail from beam column deflection response*. Washington, DC: American Railway Engineering Association (AREA), 1987, pp.280–301.
40. Otter DE, LoPresti JA and Sweeney RA. Longitudinal forces in bridges due to heavy haul freight operations. In: *Proceedings of the 7th international heavy haul association conference*. Brisbane, Australia, 10–14 June 2001. p. 4. IHHA: Virginia Beach, VA.
41. Dersch M, Roadcap T, Edwards JR, et al. Investigation into the effect of lateral and longitudinal loads on railroad spike stress magnitude and location using finite element analysis. *Eng Fail Anal* 2019; 104: 388–398.
42. Sadeghi J and Askarinejad H. Development of improved railway track degradation models. *Struct Infrastruct Eng* 2010; 6: 675–688.
43. Sharma S, Cui Y, He Q, et al. Data-driven optimization of railway maintenance for track geometry. *Transp Res Part C Emerg Technol* 2018; 90: 34–58.
44. Roadcap T, Dersch MS and Edwards JR. *Mechanistic investigation of timber crosstie spike fastener failures – phase I: the magnitude of the spike failure challenge*. DOT/FRA/ORD, Washington, DC, USA: US Department of Transportation, Federal Railroad Administration, In review.
45. Roadcap T, Dersch M and Edwards JR. Load environment and force transfer in railway fastening systems: a case study of the broken spike mystery. In: *Proceedings of the 2019 world congress on railway research*, Tokyo, Japan, 28 October–1 November 2019.
46. Edwards JR, Dersch MS and Kernes RG. *Improved concrete crosstie and fastening systems for US high speed passenger rail and joint corridors – project summary Report (Volume 1)*. Technical Report DOT/FRA/ORD-17/23, Washington, DC: US Department of Transportation, Federal Railroad Administration, 2017.
47. Talbot AN. Progress report of the special committee on stresses in track. In: *Proceedings of the American Railway Engineering Association (AREA)*. Washington, DC: American Railway Engineering Association (AREA), 1918, pp.875–1058.
48. Winkler E. *Theory of elasticity and strength*. Prague: Dominicus, 1867.
49. Zimmermann H. *Die berechnung des eisenbahnoberbaues (the analysis of railway tracks)*. 3rd ed. Berlin, Germany: Verlag W. Ernst & Sohn, 1941.
50. Van Dyk BJ, Edwards JR, Dersch MS, et al. Evaluation of dynamic and impact wheel load factors and their application in design processes. *Proc IMechE, Part F: J Rail and Rapid Transit* 2017; 231: 33–43.
51. Van Dyk BJ, Scheppe AJ, Edwards JR, et al. Methods for quantifying rail seat loads and a review of previous

experimentation. *Proc IMechE, Part F: J Rail and Rapid Transit* 2016; 230: 935–945.
52. Cho S, Lee K-C, Jang SY, et al. Sequential track–bridge interaction analysis of quick-hardening track on bridge considering interlayer friction. *Appl Sci* 2020; 10: 5066.
53. Icke P and Paice G. Track-structure interaction analysis using FE modelling techniques. In: *Proceedings of the international conference on road and rail infrastructure CETRA. Spilt dalmatia*. Croatia: University of Zagreb, 2014, p. 8.
54. Trizotto M, Dersch MS, Edwards JR, et al. Analytical elastic modeling of rail and fastener longitudinal response. *Transp Res Rec J Transp Res Board* 2021; 14: 1–14.
55. Van MA. *Stability of continuous welded rail track*. Doctoral Thesis, Technische Universiteit Delft, https://repository.tudelft.nl/islandora/object/uuid%3Acf107693-5eed-410b-a879-450aec6ec383. (1997, accessed 16 July 2021).
56. Sadeghi J and Barati P. Evaluation of conventional methods in analysis and design of railway track system. *IJCE Int J Civ Eng* 2010; 8: 44–56.
57. Dick T and Ruppert Jr C. *Mixed Freight and Higher-Speed Passenger Trains: Framework for Superelevation Design*. DOT/FRA/ORD-19/42, Washington, DC: Federal Railroad Administration (FRA), 2019.
58. Boardman, B. 1990. Fatigue Resistance of Steels, In: *ASM Handbook, Volume 1: Properties and Selection: Irons, Steels, and High-Performance Alloys*. ASM International. pp.673–688.
59. Federal Railroad Administration (FRA) Part 213 – track safety standards. In: *Title 49 of the code of federal registrations*. Washington, DC: US Department of Transportation, Federal Railroad Administration, www.gpo.gov/fdsys/granule/CFR-2011-title49-vol4/CFR-2011-title49-vol4-part213 (2011, accessed 1 November 2018).
60. American Railway Engineering and Maintenance-of-Way Association (AREMA). Ties (Chapter 30). In: *Manual for railway engineering* (ed. AREMA). Landover, MD: The American Railway Engineering and Maintenance-of-Way Association, 2017.
61. Railway applications – Track – Performance requirements for fastening systems – part 2: fastening systems for concrete sleepers. In: *European Standard (EN 13481)*. Brussels, Belgium: European Committee for Standardization (CEN), 2002.
62. Kerchof B. Effects of superelevation and speed on vehicle curving in heavy axle load service. In: WRI 2016. Chicago, IL, May 2016.
63. Dersch MS, T, Silva M, Edwards JR, et al. Analytical method to estimate railroad spike fastener stress. *Res Rec J Transp Res Board* 2020; 2674: 11.
64. Gao Y and LoPresti J. *Interim report broken spike remediation. Technology digest TD-20-004*. Pueblo, CO: Transportation Technology Center, Inc., April 2020.
65. Forest Products Laboratory. *Wood handbook, wood as an engineering material*. Centennial Edition. Madison, WI: United States Department of Agriculture, Forest Service, 2010.
66. Dersch MS, Khachaturian C and Riley Edwards J. Methods to mitigate railway premium fastening system spike fatigue failures using finite element analysis. *Eng Fail Anal* 2021; 121: 105160.